Composite organic-inorganic butterfly scales: Production of photonic structures with atomic layer deposition

Davy P. Gaillot,[1,*] Olivier Deparis,[2] Victoria Welch,[2] Brent K. Wagner,[3] Jean Pol Vigneron,[2] and Christopher J. Summers[1]

[1]*School of Materials Science and Engineering, Georgia Institute of Technology, Atlanta, Georgia 30332-0245, USA*
[2]*Laboratoire de Physique du Solide, Facultés Universitaires Notre-Dame de la Paix, B-5000 Namur, Belgium*
[3]*Georgia Tech Research Institute, Atlanta, Georgia 30332, USA*

Recent advances in the photonics and optics industries have produced great demand for ever more sophisticated optical devices, such as photonic crystals. However, photonic crystals are notoriously difficult to manufacture. Increasingly, therefore, researchers have turned towards naturally occurring photonic structures for inspiration and a wide variety of elaborate techniques have been attempted to copy and harness biological processes to manufacture artificial photonic structures. Here, we describe a simple, direct process for producing an artificial photonic device by using a naturally occurring structure from the wings of the butterfly *Papilio blumei* as a template and low-temperature atomic layer deposition of TiO_2 to create a faithful cast of the structure. The optical properties of the organic-inorganic diffraction structures produced are assessed by normal-incidence specular reflectance and found to be well described by multilayer computation method using a two-dimensional photonic crystal model. Depending on the structural integrity of the initially sealed scale, it was found possible not only to replicate the outer but also the inner and more complex surfaces of the structure, each resulting in distinct multicolor optical behavior as revealed by experimental and theoretical data. In this paper, we also explore tailoring the process to design composite skeleton architectures with desired optical properties and integrated multifunctional (mechanical, thermal, optical, fluidic) properties.

PACS number(s): 42.66.−p, 42.70.Qs, 78.20.−e

INTRODUCTION

Due to ongoing growth in the optoelectronics industry and specifically the current drive to develop light-based computer chips, there is a high demand for light manipulating devices, such as photonic band-gap materials (photonic crystals). Accordingly, extensive efforts have been made to produce suitable materials, but, this has proved to be technically very difficult (e.g., Ober [1]). In the natural world, by contrast, color producing structures and optical devices such as diffraction gratings, multilayer reflectors and photonic crystals are found in a wide variety of living organisms [2], from marine polychaete worms [3], to birds [4], and fruit [5] to beetles [2,6]. Recently, therefore, several attempts have been made to use and investigate biological materials and bioassembly methods to create artificial photonic materials [7]. Although these technologies are promising, they often involve fairly long or complicated processes.

The swallowtail family of butterflies (Lepidoptera, Papilionidae)—so called on account of the tail-like elongations to their hindwings—are particularly renowned for their striking coloration and several papilionid species are known to have color-producing structures [8–11]. One especially good example is found in the wings of the green swallowtail butterfly, *P. blumei*: an Indonesian species with a broad, strongly iridescent green stripe across its forewings and hindwings and a blue iridescence from the tail region of its hindwings [Fig. 1(a)]. The aims of this work were to deposit thin optically transparent TiO_2 layers onto the wing scales of

the butterfly *P. blumei* by low-temperature atomic layer deposition (ALD), to study the dependence of the optical properties on dielectric structure and to evaluate the potential of this simple and direct technique for designing composite multicolor reflectors and photonic devices.

BUTTERFLY ULTRASTRUCTURE AND INFILTRATION

Like other butterflies' wings [10], those of *P. blumei* are covered with millions of ~100 μm long scales. Low-
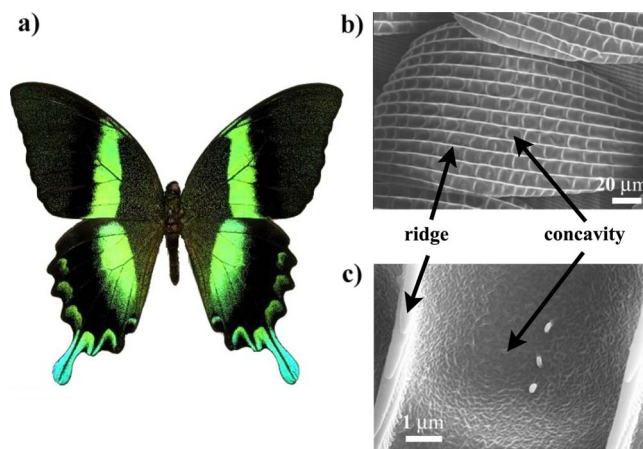

FIG. 1. (Color online) (a) Tropical *P. blumei* butterfly found in Indonesia. The wings present green iridescence bands, whereas the tail color is blue. (b) Low-magnification SEM image of the scale of a *P. blumei* butterfly. (c) The scale is composed of 5–10 μm concavities or bowls separated by chitin ridges.
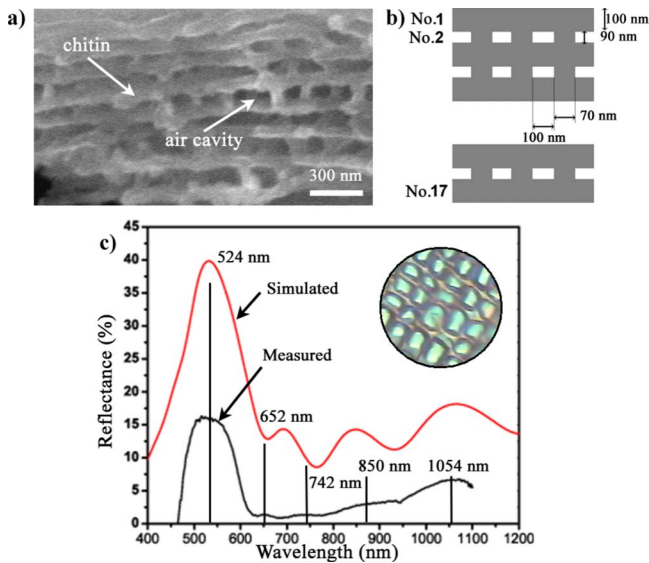
*davy@gatech.edu

FIG. 2. (Color online) (a) High-magnification SEM image of the transverse cross section of the *P. blumei* scale. The scale consists of a 17-layer air-chitin stack. (b) 2D model used for the simulations of the uncoated *P. blumei* scale. The structural parameters were determined from transverse cross sections such as (a). The scale comprises eight air layers and nine chitin layers for a total of 17 layers. (c) Comparison between measured and simulated reflectance spectra of an uncoated scale of a *P. blumei* butterfly. A ~524 nm peak is observed and predicted and is responsible for the green color of the wing. Four peaks at 652, 742, 850, and 1054 nm were observed and well matched by theory. However, the predominant effect is from the 524 nm peak. The inset shows a CCD image of an array of green-iridescent concavities taken at a 40× magnification.

magnification secondary electron microscopy (SEM) images reveal that each scale consists of an ordered array of concavities or bowls, 5–10 μm in diameter, as shown in Figs. 1(b) and 1(c). Previous investigations of this butterfly [12,13] have revealed that at higher magnification, each scale is composed of nanometer-sized rectangularly shaped air chambers separated by transverse and longitudinal laminae made of the semitransparent biological polymer chitin (refractive index $n \sim 1.52$); this structure is shown in Fig. 2(b) [12]. Since our preliminary SEM images [Fig. 2(a)] and those previously presented indicate that the scales are sealed, two infiltration schemes are possible. In the first scenario—defined here as mode I—a thin skin is conformally coated over and around the scales (but the interior left uncoated), as shown in Fig. 3(a), whereas in mode II [Fig. 5(a)] it is suggested that the air cavities can also be infiltrated through surface microcracks.

SIMULATIONS

The optical reflectance of the uncoated and conformally coated scales (mode I and mode II) was computed by a multilayer computation method based on the two-dimensional (2D) structural model developed by Tada to describe this butterfly's iridescence and used here to mimic both of the conformal deposition schemes faithfully [12]. [Note that a more refined model that includes the effect of

the thin film curvature (due to the scales' concavities) on the optical response and plane polarization effects has been presented by Vukusic *et al.* [14]]. The simulation methodology is as follows: (1) The actual scale structure is represented by a 2D photonic crystal whose structural parameters were determined from the high-magnification SEM image of the scale cross section shown in Fig. 2(a); (2) layers with air cavities are replaced by homogeneous ones using effective index approximation; (3) the resulting one-dimensional (1D) photonic crystal is modeled as an effective thin film using multilayer computation technique. The thin-film consists of a stack of eight air-chitin layers, thickness $d_2 = 90$ nm, and nine chitin layers, thickness $d_1 = 100$ nm; the transverse dimensions of air cavities and chitin are $D = 100$ and $d = 70$ nm, respectively. Consequently, a ~59% filling fraction of air, given by $f_{air} = D/(d+D)$, was computed from this model in agreement with Fig. 2(a). A complex refractive index $n(\lambda) + ik(\lambda)$ was used to simulate the dispersive optical properties of chitin. An empirical linear approximation was employed for the index dispersion with $n = 1.5$ and $k = 0.06$ at 400 nm whereas $n = 1.8$ and $k = 0.03$ at 800 nm; values retrieved from the literature [15]. Here, the effect of absorption (k) is included to reduce the intensity of the reflectance peaks and oscillations to reproduce with high fidelity the experimental measurements. In addition, the dispersive nature of amorphous TiO_2 from the uv to the near-blue regions was included in the model. Uniform averaging the reflectance spectra over the incidence angles, from $-60°$ to $+60°$ as estimated from various SEM images of bare scales, was also added as a means to simulate the effect of the concavities curvature. Note that a nonuniform averaging scheme may also be implemented but was not used in the present work because fairly good agreement was reached between the simulated and measured data.

EXPERIMENTAL ANALYSIS

The 5 mm × 5 mm square-shaped samples were cut from the *P. blumei* wing using a razor blade and placed into a custom-built ALD reactor. (Note that the wingspan of the *P. blumei* butterfly is ~10 cm.) The conformal and progressive deposition of amorphous TiO_2 was performed by low-temperature ALD at 100 °C [16]. A total thickness of 50 nm was achieved by sequentially depositing 10 nm of TiO_2 at a growth rate of 0.075 nm/cycle. Additionally, scales coated with intermediary thickness values were fabricated to obtain an additional set of samples with coatings ranging from 0 to 50 nm. Consequently, it was possible to optically assess all fabricated samples under the same experimental conditions. Normal incidence specular reflectance measurements from the bare and as-deposited scales were performed between 400–1100 nm. In addition, at each stage, the change in the architecture was monitored by SEM analysis. This adds crucial information such as the deposited TiO_2 thickness, roughness of the surface and degree of infiltration of the air-chitin stack. For the optical measurements, a 40× objective was used to obtain a focused spot size of 50 μm to minimize the long-range curvature of the scale and eliminate undesired optical perturbations from adjacent scales. This ap-
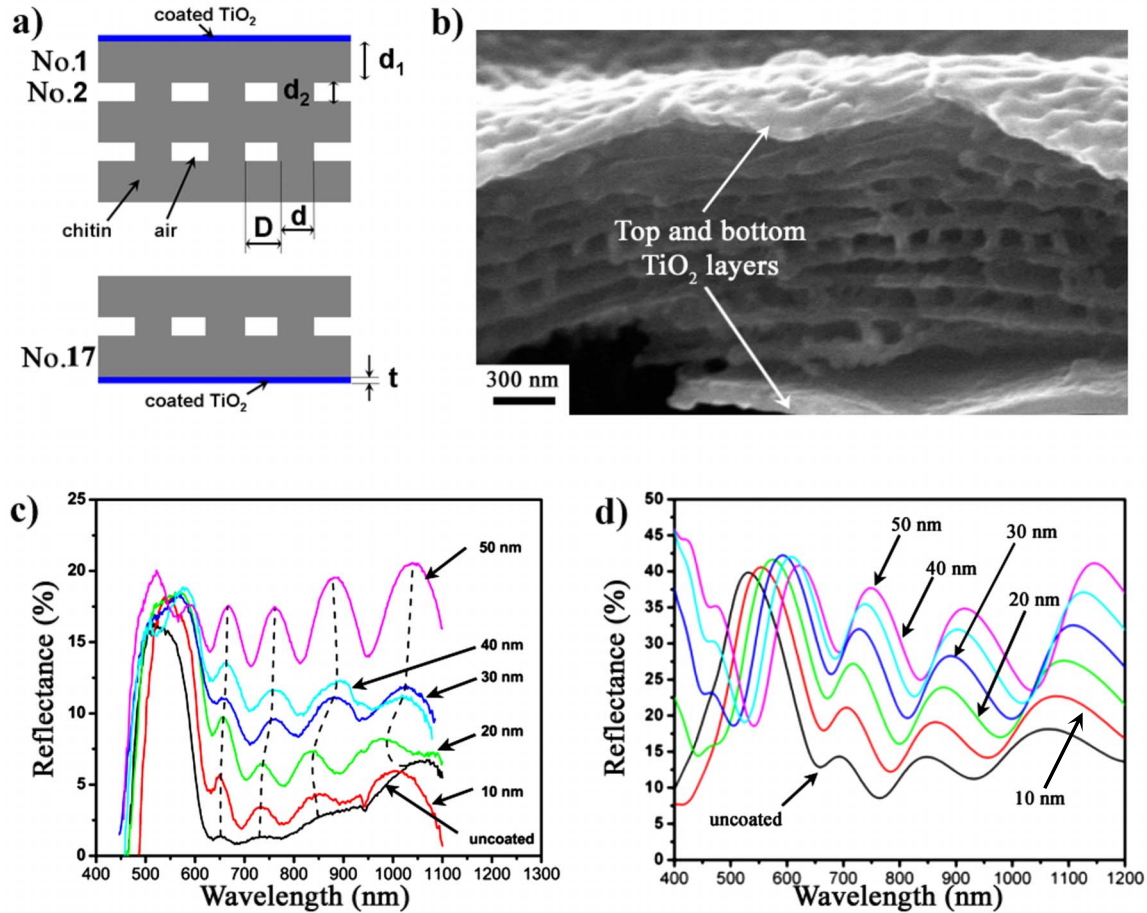
FIG. 3. (Color online) (a) 2D model used to simulate the hermetic *P. blumei* scale coated externally by ALD (mode I). TiO_2 (n_{TiO_2} =2.31) is only deposited on the top and bottom of the scale. (b) High-magnification SEM image of the cross section of a composite scale with 50 nm of TiO_2. The cleave was performed after the infiltration to reveal the unmodified air-chitin stack. (c) and (d) present the measured and simulated reflectance spectra of composite scales processed with 10, 20, 30, 40, and 50 nm of amorphous TiO_2, respectively. The dotted lines indicate the evolution of the peak position with increasing thickness.

proach was essential to assess the optical properties of the scales for normal incidence. Also note that the intensity of the spectra was normalized with respect to the intensity of the spectrum obtained with an aluminum-coated glass. In this configuration, the probed surface typically encompasses $\sim$10 concavities with a fractional reflectivity estimated to be 0.36, as reported by Tada *et al.* [12]. This value indicates that 36% of the surface contributes to the interference effect. In addition, a CCD camera was mounted on a 4.5$\times$ binocular microscope to examine the long-range color uniformity of the bare, 10, 20, 30, 40, and 50 nm deposited samples.

RESULTS AND DISCUSSION

Mode I: Externally coated scheme

Figure 2(c) presents the measured and simulated reflectance spectrum of the uncoated sample between 400 and 1100 nm, respectively. The measured spectrum is dominated by a well-defined peak centered at 524 nm which was attributed to optical interference resulting from the interaction of the incident light with the air-chitin stack. Additionally, four peaks were observed at longer wavelengths located at 652,

742, 850, and 1054 nm, respectively, thus spanning the entire spectrum. Due to their very weak intensity, these peaks make a minimal contribution to the far-field green iridescence observed at normal incidence. This measurement was repeated for each one of the bare samples studied in the present study and the results revealed a strong uniformity; as is characteristic of butterfly scales. Finally, the presence of O-H groups within the biological material may be responsible for the small absorption notch located at 944 nm since the reference spectrum procedure removes this well-known signature from our uv-vis fiber optic. Nevertheless, this small accident is not really important for the analysis of the sample. The simulated spectrum also comprises one main component located at 532 nm and four additional peaks at 596, 692, 848, and 1064 nm, thus in good agreement with the measured ones. In addition, theory also predicts a gradual increase in the intensity of the peaks with increasing wavelengths. It is noteworthy that the simulated intensity baseline is much higher than the measured one which may be due to the fact that the 2D model does not incorporate all the scattering surfaces that are really present in a complete butterfly wing.

Following this baseline calibration, the scales were sequentially coated with 10 nm of amorphous TiO_2 by low-
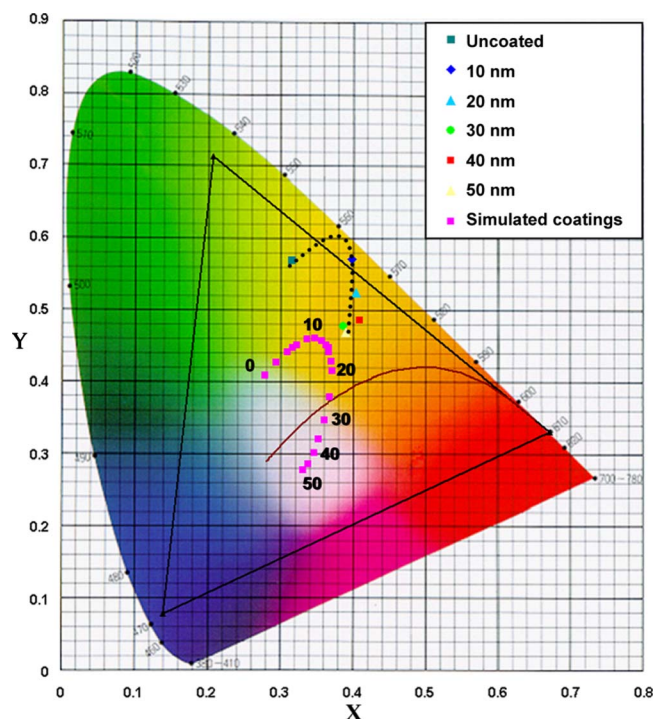
FIG. 4. (Color online) CIE 1931 color map presenting the measured and simulated monochromatic response of TiO_2-coated samples with thicknesses varying between 0 and 50 nm. The X and Y coordinates were determined from the measured (0, 10, 20, 30, 40, and 50 nm fitted by the dotted line) and simulated (0, 2, 4, 6, 8, 10, 12, 14, 16, 18, 20, 25, 30, 35, 40, 45, and 50 nm) spectra between 400 and 1100 nm.

temperature ALD, as depicted in Fig. 3(a). In the cross section of a 50-nm-coated scale, presented in Fig. 3(b), the high-magnification SEM image unambiguously demonstrates the high quality, surface smoothness and conformality of the deposited dielectric films and furthermore indicates that no additional short- or long-range structural disorder was introduced. Figure 3(c) shows the measured reflectivity spectra of the samples coated with 10, 20, 30, 40, and 50 nm of amorphous TiO_2. It was observed that the 524, 652, and 742 nm peaks progressively redshift at a rate of $\sim$1 nm per nm of TiO_2, whereas the positions of the peaks located at 850 and 1054 nm alternatively redshift and blueshift with increasing TiO_2. A key feature is the increase in the oscillation intensity and width of the longer wavelength peaks with deposition. Visual inspection of the processed samples by the naked eye or aided by a binocular microscope shows that the initial green color was progressively attenuated to paler nuances. This optical effect can be explained by the fact that the human eye displays a tristimulus response to primary colors (blue, green, and red) and averages a multicolor spectrum into a monochromatic color. The chromaticity is dependent on the intensity and frequency location of the spectral components and can be positioned in a 2D color map using coordinates X and Y as defined by the CIE 1931 convention [17]. The CIE 1931 color map shown in Fig. 4 presents the monochromatic color determined from the measured spectra (uncoated, 10, 20, 30, 40, and 50 nm) between 400 and 1100 nm. The results confirm the color variation observed at

the naked eye with increasing infiltration and also indicate that thin TiO_2 layers (from 0 to 10 nm) suffice to modify the reflected color from green to yellow-green. The effect of depositing thicker layers is to progressively shift this color towards the white portion of the map. Furthermore, the samples behave optically to the eye as broadband reflectors whose efficiency is determined by the baseline intensity of the spectrum. This effect is particularly pronounced for the 50-nm-coated-only sample from which an average intensity level of $\sim$16% was computed. The intensity and chromaticity of the reflected light can, therefore, be adjusted simply by tuning the TiO_2 coating thickness; thus this process could be developed to produce photonic structures tailored to desired optical signatures. Further, the high refractive index of TiO_2 compared with biological compounds allows for the creation of structures with properties beyond those possible with purely natural materials.

The theoretical dependence of the reflectance on the coating thickness is presented in Fig. 3(d). The oscillation patterns, peak shift, intensity, and peak width are in very good agreement with the data. All peaks progressively shift to longer wavelengths and are attenuated in intensity with increasing deposition, in contrast with the measured data where the intensity of the peaks increases. Figure 4 also includes the monochromatic color determined from several simulated spectra (0, 2, 4, 6, 8, 10, 12, 14, 16, 18, 20, 25, 30, 35, 40, 45, and 50 nm) between 400 and 1100 nm. Their chromatic position is shifted to a much whiter color compared to the measured data which originates from the difference in the intensity of their peaks at lower (due to the detector cutoff) and longer wavelengths. Again, the latter may be due to the absence of all the scattering surfaces in the 2D model. On the other hand, the evolution in the chromaticity with increasing deposition, depicting a portion of an ellipse, is in good agreement with the measured data; thus supporting the effectiveness of the model.

The measured and simulated patterns display spectral characteristics very typical to those observed from Fabry-Perot optical cavities. Hence, in the organic-inorganic sandwich structure studied, the high-index bottom and top TiO_2 layers, which behave as reflective mirrors, are responsible for the formation of additional reflected modes. More importantly, the results demonstrate that the precise control over the mirror thickness by ALD enables the finesse or quality factor of the hybrid etalon to be finely tuned and enhanced with subsequent chromatic adjustments. To the knowledge of the authors, this effect has never previously been explored or reported.

Mode II: Internally and externally coated scheme

In the second scheme, we suggest that the ALD gas precursors can diffuse within the porous stack through surface microcracks and fissures. Consequently, thin dielectric layers can not only be conformally deposited around and over the scale body but also onto the interior of the chitin walls, as depicted in Fig. 5(a). Although, cracks can be realized by the means of a sharp tip, the scales located at the edge of the samples can be unintentionally cracked during the sampling
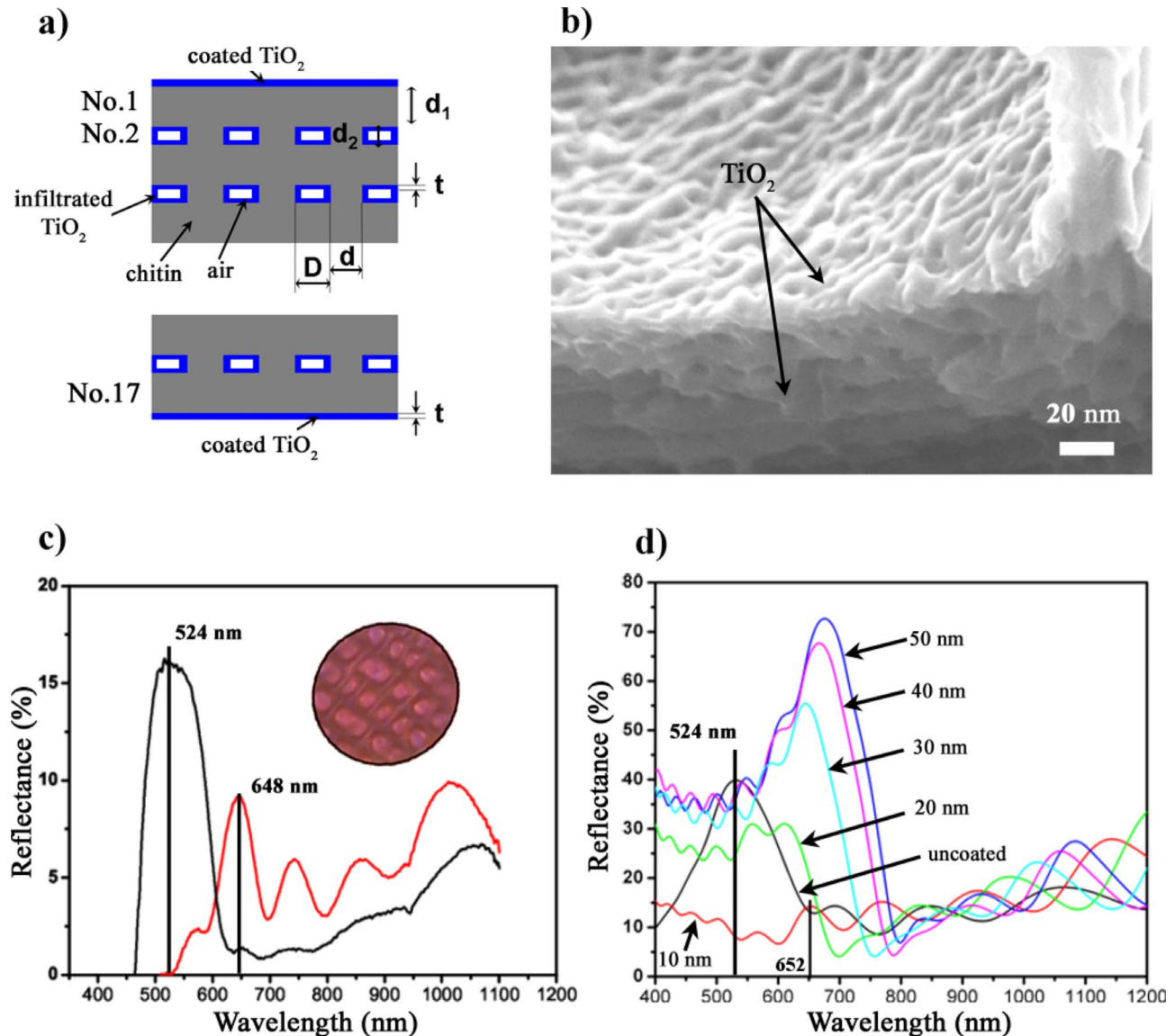
FIG. 5. (Color online) (a) 2D model used to simulate the fractured *P. blumei* scale coated both internally and externally by ALD (mode II). TiO$_2$ is deposited on the top and bottom of the scale and also onto the interior of the chitin walls. (b) High-magnification SEM image of the cross section of a coated scale with 30 nm of TiO$_2$. (c) and (d) present the measured (10 nm) and simulated (between 10 and 50 nm) reflectance spectra of coated scales processed with amorphous TiO$_2$, respectively. The predominant peak shifts from 524 to 648 nm with 10 nm of TiO$_2$ in good agreement with the simulations (652 nm). The inset shows a CCD image of an array of red-iridescent concavities taken at 40× magnification.

procedure using a razor blade or during handling with tweezers. Visual examination of the sample coated with 10 nm of TiO$_2$ reveals the presence of bright red scales sparsely distributed at the edge. The color change from green [inset Fig. 2(c)] to red [inset Fig. 5(c)] over the whole surface of the scale indicates that the surface was cracked-open before the infiltration procedure. Moreover, the uniform color change shows that homogeneous infiltration was achieved, and adds critical knowledge to the internal architecture of the scale. For instance, it indicates that the air cavities form a fully interconnected network: an experimental finding that can be used to improve the present optical model (in which separated air cavities were assumed) or to extend it to a three-dimensional (3D) photonic crystal model, such as those re-

ported in other organisms—e.g., an iridescent weevil [6]. The optical properties of the scales were then characterized and Figs. 5(c) and 5(d) present the measured and simulated reflectance spectrum of uncoated and 10-nm-coated-infiltrated scale. In contrast with the externally coated structure, the 524 nm peak is observed to shift to 648 nm, in good agreement with the simulations performed with a modified 2D model. In addition, the intensity of this peak is strongly attenuated whereas the intensity of the lower-order peaks is enhanced, as explained earlier. The large 122 nm shift in the central peak is here attributed to the reduction in the filling fraction of air from ~59% to ~37%, and subsequent increase in the effective index of the infiltrated stack. The simulations performed for 20, 30, 40, and

50 nm coatings [Fig. 5(d)] clearly show the progressive shift, broadening, and intensity increase of the main peak. This well-known effect has been widely described in the literature for low-index porous networks conformally infiltrated by a high-index material including synthetic opals [16,18], holographically defined templates [19], and more recently biological species [20].

CONCLUSION

Thin amorphous layers of TiO_2 were conformally deposited onto and into the scales of a *P. blumei* butterfly by low-temperature ALD. Depending on the air-chitin stack accessibility, two infiltration schemes were identified resulting in distinct optical responses. The first, sandwiching the sealed original template with partially reflecting TiO_2 mirrors yielded the formation of a unique hybrid organic-inorganic Fabry-Perot etalon whose finesse, spectral component intensity, and monochromatic coloration were precisely controlled by the deposited thickness. Thus, it was shown that in the second scheme, this effect might occur simultaneously with the effect resulting from the manipulation of the internal air network. This provided additional flexibility to the tuning of the original optical properties, which were adjusted to a different spectral region. In addition to the above, the ALD tool indirectly revealed the structural complexity of the multilayer scale in the *P. blumei* butterfly, which is more complex than had previously been realized, with interconnecting air chambers. The method presented in this study, then, offers an alternative route for designing and producing bioinspired materials with unique optical properties.

Finally, we note that biological color producing structures have often evolved to satisfy several competing sets of demands (evolutionary pressures): A butterfly wing scale, for example, must be simultaneously aerodynamically shaped, structurally strong, lightweight and endowed with many fluidic and thermal [21] properties, as well as the optical behavior described. By using such structures as templates, it may be possible to produce photonic devices which retain some of these other desirable properties, as well as the optical faculties required.

ACKNOWLEDGMENTS

[1] C. K. Ober, Science **296**, 859 (2002).

[2] A. R. Parker, J. Exp. Biol. **201**, 2343 (1998).

[3] A. R. Parker, R. C. McPhedran, D. R. McKenzie, L. C. Botten, and N. A. P. Nicorovici, Nature (London) **409**, 36 (2001).

[4] V. L. Welch and J. P. Vigneron, Opt. Quantum Electron. **39**, 295 (2007).

[5] D. W. Lee, Nature (London) **349**, 260 (1991).

[6] V. Welch, V. Lousse, O. Deparis, A. Parker, and J. P. Vigneron, Phys. Rev. E **75**, 041919 (2007).

[7] A. R. Parker and H. E. Townley, Nat. Nanotechnol. **2**, 347 (2007).

[8] S. Berthier, *Iridescences: les couleurs physiques des insectes* (Springer, Paris, 2003).

[9] J. Huxley, Proc. R. Soc. London, Ser. B **193**, 441 (1976).

[10] S. Kinoshita and S. Yoshioka, *Structural Colors in Biological Systems: Principles and Applications* (Osaka University Press, Osaka, 2005).

[11] P. Vukusic and R. Sambles, *Physics, Theory, and Applications of Periodic Structures in Optics, 2001* (International Society for Optical Engineering, San Diego, CA, 2001), p. 85.

[12] H. Tada, S. E. Mann, I. N. Miaoulis, and P. Y. Wong, Opt. Lett. **5**, 87 (1999).

[13] P. Vukusic, R. Sambles, C. Lawrence, and G. Wakely, Appl. Opt. **40**, 1116 (2001).

[14] P. Vukusic, J. R. Sambles, and C. R. Lawrence, Nature (London) **404**, 457 (2000).

[15] S. Berthier, E. Charron, and A. Da Silva, Opt. Commun. **228**, 349 (2003).

[16] J. S. King, E. Graugnard, and C. J. Summers, Adv. Mater. (Weinheim, Ger.) **17**, 1010 (2005).

[17] N. Otha and A. R. Robertson, *Colorimetry—Fundamentals and Applications* (Wiley, Chichester, 2005).

[18] F. Garcia-Santamaria, M. Ibisate, I. Rodriguez, F. Meseguer, and C. Lopez, Adv. Mater. (Weinheim, Ger.) **15**, 788 (2003).

[19] J. S. King, E. Graugnard, O. M. Roche, D. N. Sharp, J. Scrimgeour, R. G. Denning, A. J. Turberfield, and C. J. Summers, Adv. Mater. (Weinheim, Ger.) **18**, 1561 (2006).

[20] J. Huang, X. Wang, and Z. L. Wang, Nano Lett. **6**, 2325 (2006).

[21] L. P. Biró *et al.*, Phys. Rev. E **67**, 021907 (2003).